Dynamic Response of Pile Foundations--

EXPERIMENT, ANALYSIS AND OBSERVATION

Proceedings of a session of the
Geotechnical Engineering Division of the
American Society of Civil Engineers
in conjunction with the ASCE Convention
in Atlantic City, New Jersey

April 27, 1987

Edited by Toyoaki Nogami

Geotechnical Special Publication No. 11

Published by the
American Society of Civil Engineers
345 East 47th Street
New York, New York 10017-2398

Prediction of Dynamic Lateral Response of Nonlinear Single-Pile by Using Winkler Soil Model

By Toyoaki Nogami,[1] M.ASCE, and H.-L. Chen[2]

The first author has recently proposed the dynamic nonelastic Winkler soil model and the method to define its parameters. The paper first verifies the modeling concept used in this model and examines the capability of the model of predicting the dynamic response of a single pile in the field. The test data obtained in the full-scale field pile load tests were utilized for this study. The pile responses computed by using the proposed model agrees with those observed in the field test in general.

INTRODUCTION

Various approaches have been used for the dynamic response analysis of single piles. They are characterized by the differences in the treatment of the soil medium in the analysis. The simplest of all appears to be the approach based on a Winkler soil model. Basically two types of Winkler models have been developed for the dynamic response analysis of single piles. The first type of soil models consists of the nonlinear spring and dashpot placed in parallel to each other (Voigt type model). The spring constant is defined by the so called $p-y$ curve, which describes the nonlinear force-displacement relationship of the spring, and the dashpot constant is defined from the radiation damping in an elastic medium (3). This model is widely used for the dynamic response analysis of single piles. However, in a nonlinear environment the model mechanism is not consistent with the physical conditions of the soil around the pile shaft and thus is never capable of reproducing the damping rationally (7).

The second type of Winkler soil models are those in which the parameters are defined from the dynamic behavior of a plane strain continuous medium: the plane strain conditions referred herein correspond to an infinitely long massless rigid circular cylinder embedded in an infinite medium. The elastic model of this type was developed by Novak, Nogami and Aboul-Ella (10) in the frequency-domain, and by Nogami and Konagai (9) in the time domain. The nonelastic model was developed by Nogami (7) in the frequency-domain. He also proposed the method to define the parameters of this model by using the "static cyclic" complex $p-y$ curve. The real and imaginary parts of the static cyclic complex $p-y$ curve correspond to the conventional cyclic $p-y$ curve and the curve expressing the hysteresis damping induced by the system nonelasticity, respectively.

The main purposes of this paper are to provide an example case for determining the parameters of the Winkler model proposed by the first author in Ref. 7, and to examine the capability of the proposed model of predicting the dynamic lateral response of a single pile. The previously proposed approach is modified so that the model parameters are defined by the conventional $p-y$ curve without providing the imaginary part.

DYNAMIC NONLINEAR WINKLER MODEL

The soil model proposed in Reference 7 is based on a Winkler's hypothesis. Thus the soil reaction reproduced by this model is related to the pile displacement only at the depth where the soil reaction is considered. Such an approximation is frequently used and verified for both

[1] Scripps Institution of Oceanography, University of California at San Diego, La Jolla, CA 92093

[2] Dept. of Civil Engineering, University of Houston, Central Campus, Houston, TX 77004

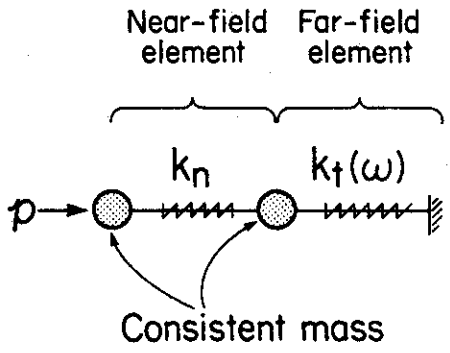

Figure 1. Proposed Dynamic Nonlinear Winkler Model

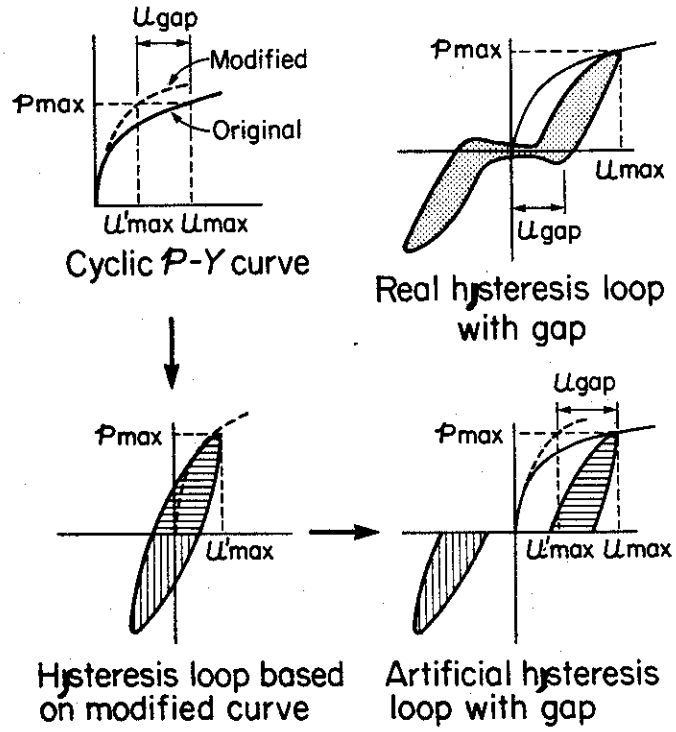

Figure 2. Artificial Hysteresis Loop with Gap

dynamic and static conditions, (i.e. 2,4,5,6,7,12).

Figure 1 shows one unit of the proposed Winkler soil model. The near-field element consists of a complex spring and consistent mass, and represents the soil in the vicinity of the pile where a strong nonlinearity is induced by the pile shaft displacement. The imaginary part stiffness of this element results from the damping due to the nonelastic behavior. The far-field element consists of a complex spring, and represents the soil outside of the area considered for the near-field element. The soil represented by the far-field element behaves more or less elastically and generates the radiation damping. The imaginary stiffness of this element results from the radiation damping. Under harmonic steady state motion, the complex stiffness of the unit as shown in Figure 1 is expressed by:

$$k(\omega) = k_n - m_{11}\omega^2 - \frac{(k_n)^2 + k_n\,\omega^2\,(m_{12} + m_{21}) + m_{12}m_{21}\omega^4}{k_n + k_f(\omega) - m_{22}\omega^2} \tag{1}$$

where ω = excitation circular frequency; k, k_n and k_f = complex stiffnesses of the Winkler model, near-field element and far-field element, respectively; and m_{11}, m_{12}, m_{21} and m_{22} = values in a consistent masses matrix located as shown in Eq. 2.

Assuming that the distance r_1 measured from the center of the pile is the extent of the soil area considered for the near-field element and that the variation of the soil displacement is linear with the distance from the pile, the consistent mass matrix is given by:

$$\begin{bmatrix} m_{11} & m_{12} \\ m_{21} & m_{22} \end{bmatrix} = \frac{\pi\rho r_o^2}{6}\left(\frac{r_1}{r_o} - 1\right)\begin{bmatrix} \frac{r_1}{r_o} + 3 & 3\frac{r_1}{r_o} + 1 \\ 3\frac{r_1}{r_o} + 1 & \frac{r_1}{r_o} + 1 \end{bmatrix} \tag{2}$$

where ρ = mass of a unit volume of the soil; and r_o = radius of the pile.

DETERMINATION OF k_n AND $k_f(\omega)$

Near-Field Element. --

Since the near-field element can reproduce dynamic effects through the consistent masses by itself, the complex stiffness of spring in this element is assumed to be independent of the frequency. Thus, by knowing k $(\omega = 0)$ and $k_f(\omega = 0)$, k_n is found from Eq 1 with $\omega = 0$. That is:

$$k_n = \frac{k(\omega = 0)\; k_f(\omega = 0)}{k_f(\omega = 0) - k(\omega = 0)} \tag{3}$$

Both the real and imaginary parts of $k(\omega = 0)$ can be defined when the "static cyclic" $p-y$ curve is given. Under a harmonic environment, the hysteresis loop in the force-displacement relationship is related to the complex stiffness k through:

$$\text{Real } k = \frac{p_{\max}}{u_{\max}} \quad \text{and} \quad \text{Imag.k} = \frac{\text{AREA}}{\pi u_{\max}^2} \tag{4}$$

where $p_{\max}$ and $u_{\max}$ = the maximum values (amplitudes) of the force and displacement, respectively; and $AREA$ = enclosed area of the hysteresis loop. A conventional cyclic $p-y$ curve is a common backbone curve for force-displacement relationship hysteresis loops at various force-amplitude levels, and thus shows the $p_{\max} - u_{\max}$ relationship. The real part of $k(\omega = 0)$ is then the secant slope of the curve. The imaginary part can be defined through a hysteresis loop determined by using the conventional cyclic $p-y$ curve and Masing's rule. However the portion of the $p-y$ curve, where the gap is formed at the soil-pile interface, needs to be modified when determining the enclosed area. This procedure is illustrated in Figure 2 in which u_{gap} is the amount of gap. The stiffness $k_f(\omega = 0)$ can also be determined from the conventional cyclic $p-y$ curve as explained later. Thus, when the conventional cyclic $p-y$ curve is provided, k_n is completely defined from Eq. 3.

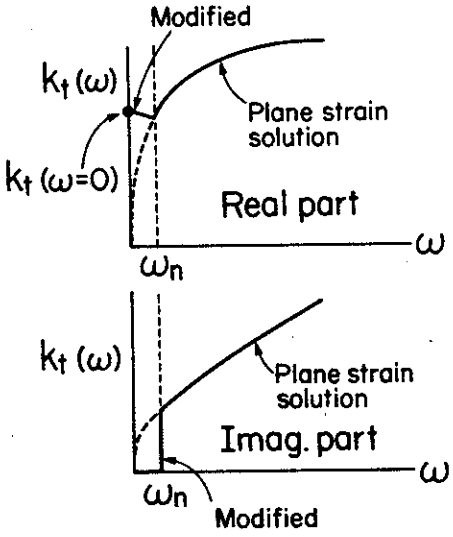

Figure 3. Variation of $k_f(\omega)$ with Frequency

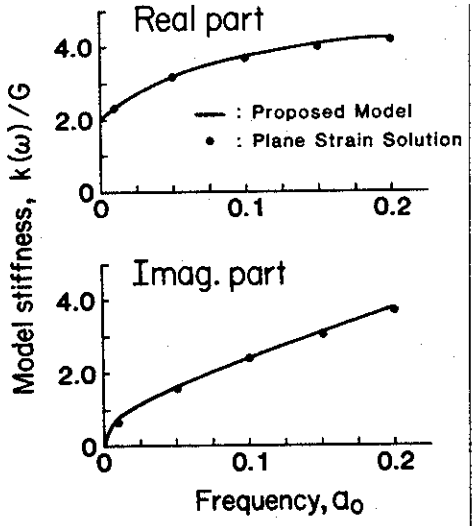

Figure 4. Check of the Proposed Model under Elastic Conditions

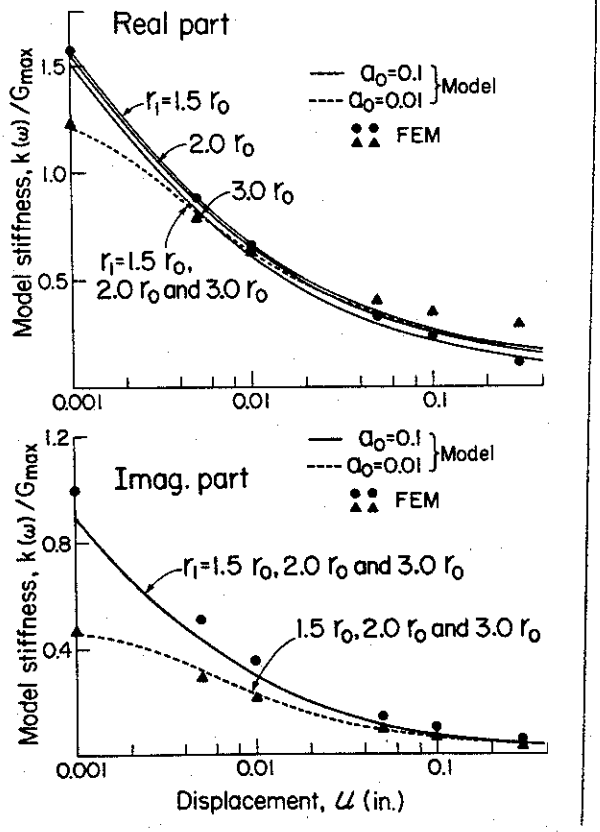

Figure 5. Check of the Proposed Model under Nonelastic Conditions

Far-Field Element. --

Since the soil represented by the far-field element behaves more or less elastically, $k_f(\omega)$ is determined from the analytical solutions developed for the vibration of a cylinder embedded in an elastic medium (Appendix I). The conditions considered are infinitely long massless rigid cylinders with a radius r_1 and an infinite elastic medium (plane strain conditions). However, this solution fails to produce reasonable values at $\omega \approx 0$. Therefore the modification is made in this frequency range as shown in Figure 3 in which ω_n may be taken as the fundamental frequency of the soil deposits at the site.

The static value $k_f(\omega = 0)$ is determined by using the following relationship:

$$\frac{1}{k_f(\omega = 0)} = \frac{u(r_1)}{p} = \frac{u(r_o)}{p} - \frac{u(r_o) - u(r_1)}{p} \tag{5}$$

where $u(r_o)$ and $u(r_1)$ = static elastic displacement of the soil at the pile and at the distance r_1 from the pile, respectively. The first term is the inverse of the initial slope of the conventional cyclic $p-y$ curve. The second term can be determined from the static solution developed for a cylinder with a radius r_o embedded in an elastic medium (Appendix I). The conditions of the cylinder and elastic medium are identical as those considered for $k_f(\omega)$.

VERIFICATION OF MODELING CONCEPT

In the proposed soil model, the soil is represented by the nonelastic near-field element and the elastic far-field element. The near-field element parameters are determined from the static conditions. In order to examine this modeling concept, studies were made for each of the elastic and nonelastic environments.

In the study for the elastic environment, the static stiffness of the near-field element was determined by using the static plane strain continuum solution, developed for a rigid cylinder embedded in an elastic medium, instead of using the cyclic $p-y$ curve. Three different sizes, $r_1 = 1.5r_o$, $2.0r_o$ and $3.0r_o$, were considered for the extent of the soil represented by the near-field element. The complex stiffnesses of the model, $k(\omega)$, were computed at various frequencies. No visible differences were observed among the results computed for various values r_1. Thus the computed results are shown only for $r_1 = 2.0\ r_o$ in Figure 4 together with those computed directly from the dynamic elastic continuum solution. The notations G and a_o in the figure are defined respectively as the soil shear modulus and $\omega\ r_o/v_s$ in which v_s is the shear wave velocity of the soil. As is seen in the figure, the model can reproduce the elastic behavior of the original medium very well for $a_o \leqslant 0.2$ and even for $a_o \leqslant 0.5$ in general.

In the study for the nonelastic environment, the static plane strain finite element method was used to determine $k(\omega = 0)$ at various displacement amplitudes first, and then k_n is defined from Eq. 3. Three different sizes, $r_1 = 1.5r_o$,$2.0r_o$ and $3.0r_o$, were considered for the extent of the soil represented by the near-field element. The nonlinear cyclic conditions are implemented through the strain amplitude dependent complex shear modulus. The computed complex stiffnesses of the model are shown in Figure 5. The complex soil stiffnesses, $k(\omega)$, were also computed directly from the dynamic plane strain finite element - boundary element method, in which the nonlinear cyclic conditions were considered in the finite element area through the strain amplitude dependent complex shear modulus. This computed results are also shown in Figure 5. Good agreement between the two results indicates that the proposed model defined from the static cyclic load can adequately reproduce the dynamic behavior of the nonelastic system. The stiffness of the model appears to be rather insensitive to the size of the soil represented by the near-field element within a practical range of the frequency.

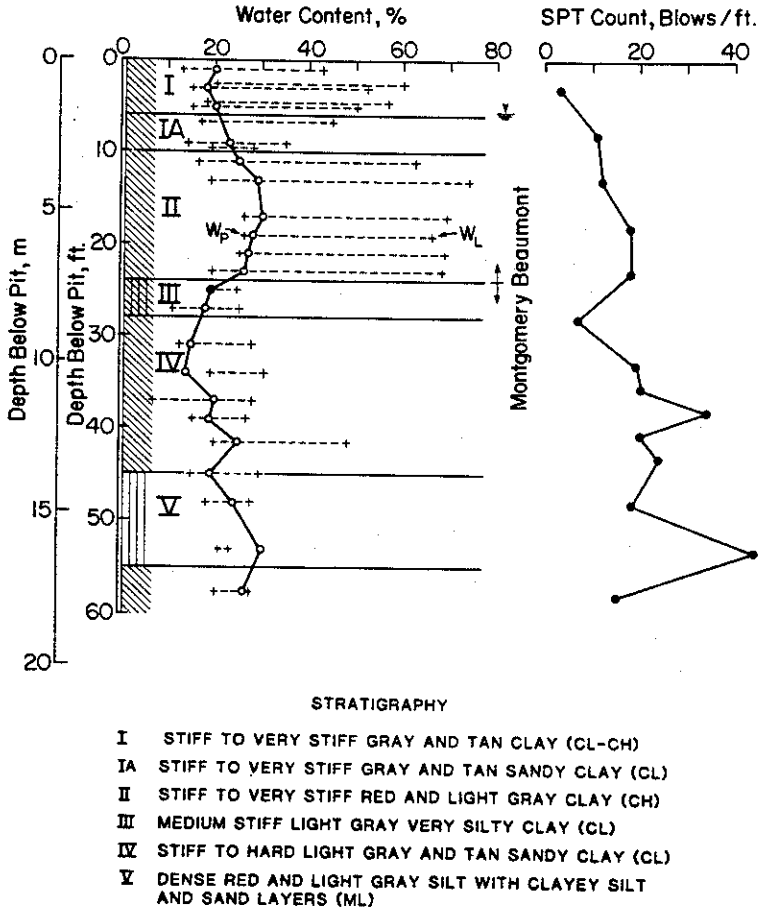

Figure 6. Soil Profile at the Test Site (Ref. 11)

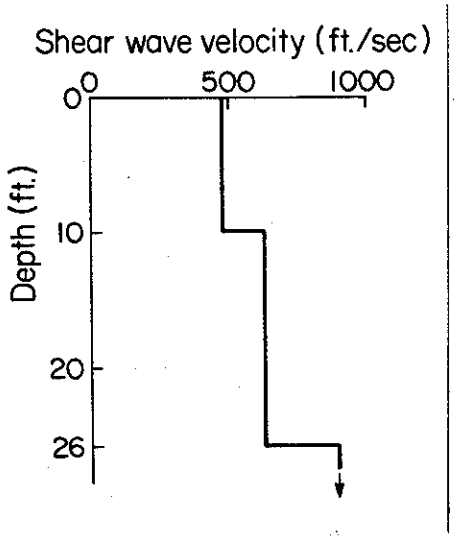

Figure 7. Distribution of Shear Wave Velocity with Depth at the Test Site (Ref. 1)

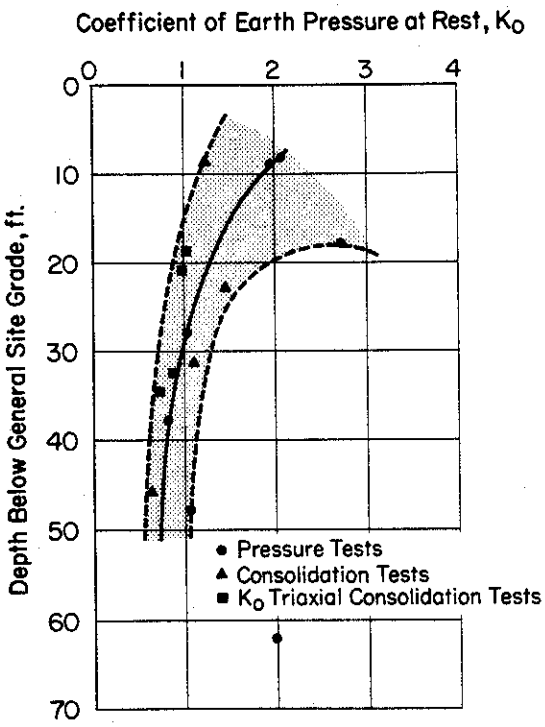

Figure 8. Distribution of K_0 Values with Depth at the Test Site (Ref. 11)

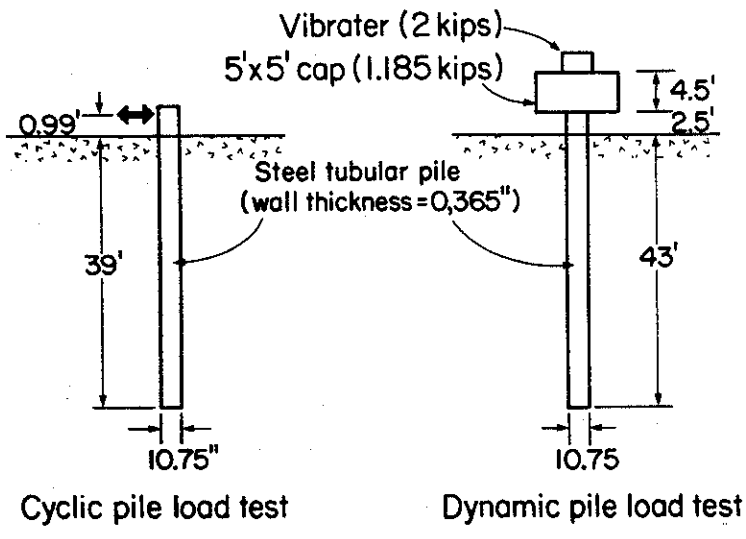

Figure 9. Cyclic Load Test and Dynamic Load Test

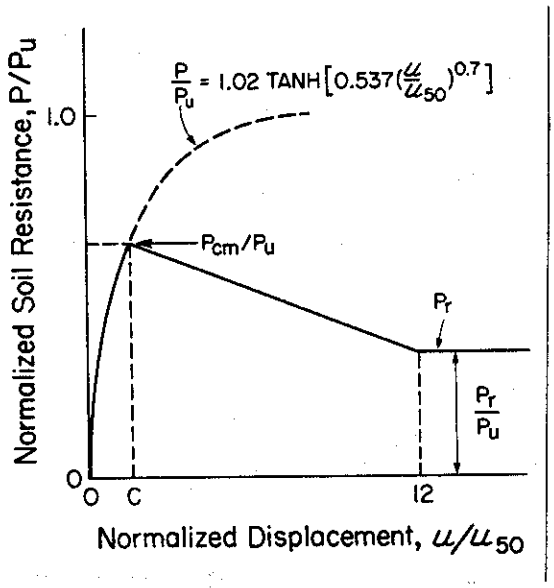

Figure 10. Cyclic p-y Curve Proposed for the U H Site (Ref. 11)

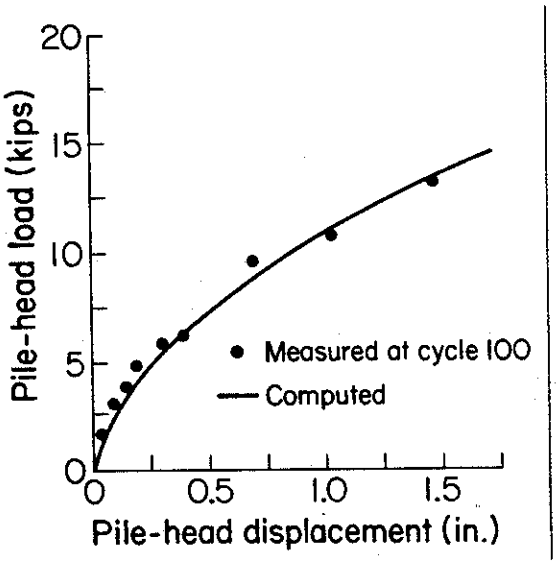

Figure 11. Computed and Measured Cyclic Displacements at the Cap

PREDICTION OF DYNAMIC RESPONSE OF A SINGLE PILE

Full-scale field tests on single piles were conducted at the University of Houston for each static cyclic load and dynamic harmonic load. Although those two different type tests were conducted independently, the properties and dimensions of the piles used in those tests were nearly identical. The parameters of the proposed model were determined from the cyclic test results following the aforementioned procedures first. The dynamic responses were predicted by using this model and the predicted values were compared with those observed in the field test to examine the present approach. The detailed information of those experiments can be found in Refs. 1 and 11.

Pile and Site Information and Field Tests. --

The soil profile at the site is shown in Figure 6. Beaumont formation covers up to about 25' from the surface and is underlain by Montgomery formation. The site is classified as a stiff clay site. The shear wave velocity profile along the depth, measured by a cross-hole seismic survey, is shown in Figure 7. The coefficient of earth pressure at rest, K_o, is shown in Figure 8.

The piles used in the tests are steel tubular piles with a wall thickness 0.365" and outside diameter 10.75". The piles used in cyclic and dynamic tests were driven to 39' and 43' depths, respectively. The lateral load was applied by the jack in the cyclic load test and by the dynamic exciter in the dynamic load test, as shown in Figure 9.

Determination of Model Parameters. --

Based on the results obtained in the cyclic test, the cyclic $p-y$ curve as shown in Figure 10 has been proposed for the test site (11). The notations used in the figure are: P_u = maximum soil resistance under monotonic load; P_{cm} = maximum soil resistance under cyclic load; P_r = residual cyclic resistant; C = normalized displacement at which the cyclic soil resistance starts to decay with increasing displacement amplitude; u_{50} = half of the displacement level corresponding to P_u. All quantities defining the $p-y$ curve can be found in Reference 11 for the test site soil.

The static pile-head displacement analyses were conducted for the monotonically applied load, treating the cyclic $p-y$ curve shown in Figure 10 as the one for the monototic load. The computed pile-head displacements were compared with those observed in the field test to make sure that this proposed $p-y$ curve can reproduce the pile-head displacement observed in the field test. It was found that the $p-y$ curve adjusted by scaling up the ordinate by 10% reproduced the observed pile-head displacements very well, as shown in Figure 11. Thus, this adjusted curve was used as the input "static cyclic" $p-y$ curve to determine the model parameters. The extent of the soil represented by the near-field element was taken as $2.0r_o$ in defining the model parameters.

The cyclic $p-y$ curve needs to be modified when the soil-pile gap effects are considered in computation of the area of the assumed hysteresis loop. For this modification, the gap is assumed to be formed when the soil resistance p is the cyclic $p-y$ curve is larger than $2\pi r_o \sigma_c$ in which σ_c is the confining pressure under K_o condition, and the amount of gap, u_{gap}, is also assumed to be:

$$u_{gap} = \beta(u-u_c) \tag{6}$$

where u_c = displacement amplitude corresponding to $p = 2\pi r_o \sigma_c$ at which the gap starts to be formed; β = empirical factor. The pile analysis with the present soil model enables one to compute not only the maximum displacement but also the hysteresis damping during the "static cyclic" response in terms of complex numbers. Thus, the hysteresis damping at the pile-head were computed by analyzing the pile response for various assumed β values. Those computed values were compared with the hysteresis damping directly computed from the observed hysteresis loop to find the reasonable value β. The hysteresis loop obtained in the field test as shown in Figure 12 was used in this study. The damping computed from this hysteresis loop is 11.5%, and those computed by the analysis with $\beta = 0$, 0.1 and 0.2 are 23.4%, 13.3% and 12.2%, respectively. This indicates that the reasonable value β appears to be approximately equal to 0.2 for the particular site and pile considered herein, and thus $\beta = 0.2$ was used for the dynamic analysis.

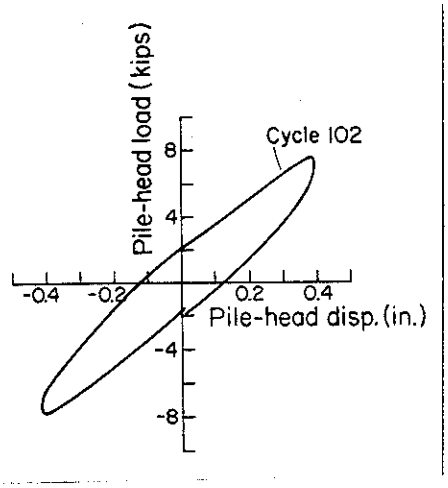

Figure 12. Force-Displacement Hysteresis Loop Measured at the Cap

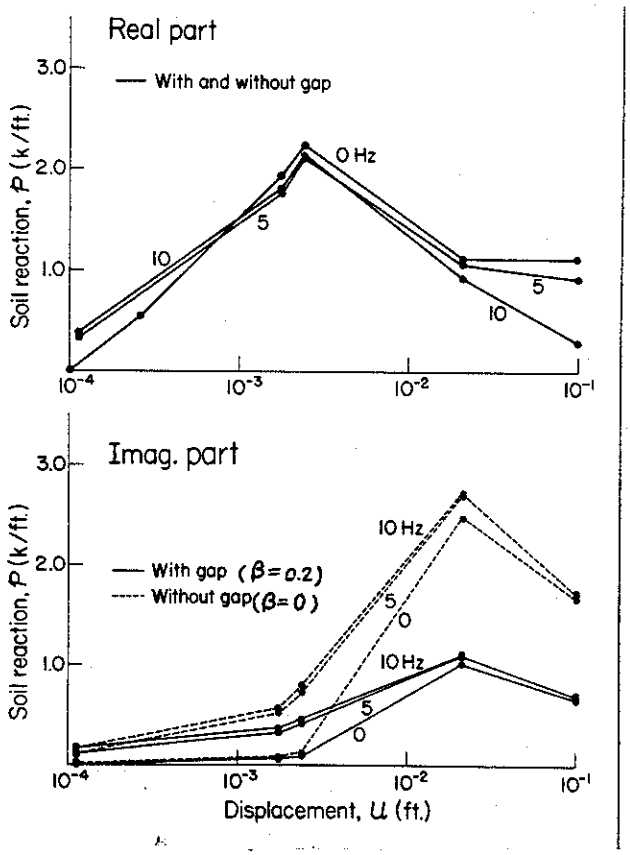

Figure 13. p-y Curve at Various Frequencies Computed by Proposed Model

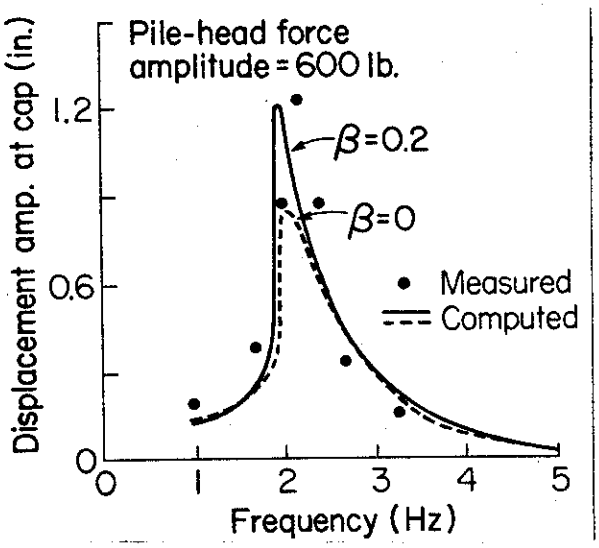

Figure 14. Displacement Amplitudes at Various Frequencies Computed and Measured at the Cap

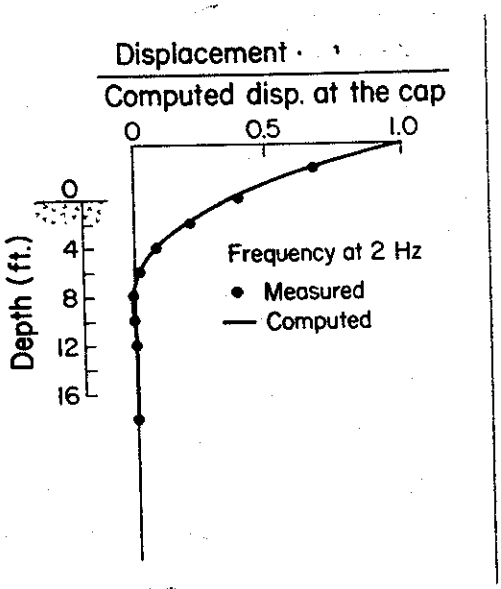

Figure 15. Computed and Measured Pile Shaft Displacement Amplitudes along the Shaft for Dynamic Load

Prediction of Dynamic Response of Pile. --

The dynamic behavior of the above defined Winkler model is first shown in Figure 13. Soil conditions used for the determination of this model correspond to those at the 3' depth from the ground surface. The dynamic behavior of the model computed by assuming $\beta = 0$ is also shown in the figure for the comparison. The real part at $a_o = 0$ in Figure 13 is identical to the input cyclic $p-y$ curve. The value in the imaginary part is proportional to the amount of the damping, which results from not only the hysteresis damping but also the radiation damping under the dynamic environment. As is seen in the figure, the gap reduces the damping rather significantly and the dynamic condition increases the damping more significantly at smaller displacement amplitudes. The latter is because the radiation damping effects are most pronounced under the elastic condition and diminishes as the nonelastic zone grows at the vicinity of the pile shaft.

Using the model defined from the static cyclic pile load test, the dynamic responses of the pile foundation were computed under the conditions identical to those in the field test. Figure 14 shows the displacement amplitudes at the cap computed for various frequencies and those observed in the field test. The computed amplitudes for $\beta = 0$ are also shown in Figure 14. Distribution of the pile shaft displacement amplitudes along the depth is shown in Figure 15 for both the computed and observed results. Those figures indicate that the proposed soil model can predict the dynamic response of a pile foundation reasonably well. It is also seen that neglecting the gap effect in determining the imaginary part of the near-field element stiffness ($\beta = 0$) leads to a lower estimation of the peak amplitude. This is due to an over-estimation of the damping by neglecting the gap effect as is seen in Figure 13.

CONCLUSIONS

The nonelastic Winkler soil model proposed for dynamic pile response analysis consists of the near-field and far-field elements. The nonlinear behavior is considered through the nonlinear near-field element. The non-linear characteristics of the element can be completely defined from the "static cyclic" $p-y$ curve. However, modification of the curve is needed to account for soil-pile gap effects in determining the imaginary part of the complex stiffness of the near-field element. The proposed soil model appears to be capable of predicting the dynamic response of the pile foundation well when the model parameters are defined by the method described in this paper. However, the present study is very limited and further experimental studies are needed to make a definite conclusion.

ACKNOWLEDGEMENT

This work has been supported by the National Science Foundation under Grant No. CEE-8310623, of which Dr. K. Thirumalai is the cognizant NSF program official. This support is gratefully acknowledged. The authors also wish to thank Dr. O'Neill of the University of Houston for allowing us to use his experimental data.

APPENDIX I--EXPRESSIONS

1. Expression for $k_f(\omega)$

$$k_f(\omega) = \pi G \left\{ 2a^2 + 4a \frac{K_1(a)}{K_o(a)} \right\} \qquad \nu = 0.5$$

$$= -\pi G a^2 \frac{4K_1(b)K_1(a) + aK_1(b)K_o(a) + bK_o(b)K_1(a)}{bK_o(b)K_1(a) + aK_1(b)K_o(a) + abK_o(b)K_o(a)} \qquad \nu \neq 0.5$$

where K_j = modified Bessel function of the second kind of order j; G and ν = shear modules and Poisson's ration of the medium, respectively; $a = i\,\omega\, r_1/v_s$; $i = \sqrt{-1}$; $b = a/\eta$; $\eta = v_p/v_s$; and v_p = P − wave *velocity*.

2. Expression for $\{u(r_o) - u(r_1)\}/p$

$$\frac{u(r_o) - u(r_1)}{p} = \frac{1}{2}\left\{ \frac{u(r_o) - u(r_1,0^\circ)}{p} + \frac{u(r_o) - u(r_1,90^\circ)}{p} \right\}$$

$$= \frac{3 - 4\nu}{8\pi G(1-\nu)} \ln \frac{r_1}{r_o}$$

where $(r_1,0^\circ)$ and $(r_1,90^\circ)$ = locations at r_1 in the direction of the horizontal load applied and the direction perpendicular to this direction, respectively.

APPENDIX II--References

1. Blaney, G. W. and O'Neill, M. W., 'Lateral Response of a Single Pile in Oversolidated Clay to Relatively Low Frequency Pile-Head Loads and Harmonic Ground Surface Loads,' Research Report UHCE 83-19, Dept. of Civil Engineering, University of Houston, 1983.

2. Matlock, H., 'Correlations for Design of Laterally Loaded Pile in Soft Clays,' Paper No. OTC 1204, Second Annual Offshore Technology Conference, Vol. 1, Houston, Texas, 1970, pp. 577-594.

3. Matlock, H., Foo, S. H. and Bryant, L.-L., 'Simulation of Lateral Pile Behavior,' Proceedings, Earthquake Engineering and Soil Dynamics, ASCE, Pasadena, California, July, 1978, pp. 600-619.

4. Nogami, T., 'Dynamic Group Effect in Axial Response of Grouped Piles,' Journal of Geotechnical Engineering Division, ASCE, Vol. 109, No. GT2, 1983, pp. 228-243.

5. Nogami, T., 'Nonlinear Dynamic Winkler Model for Lateral Cyclic Response Analysis of Single Piles,' Proceedings of the Second International Conference on Soil Dynamics and Earthquake Engineering, on board the liner the Queen Elizabeth 2, June/July, 1985, pp. 4.51-4.60.

6. Nogami, T. and Konagai, K., 'Time Domain Axial Response of Dynamically Loaded Single Piles,' Journal of Engineering Mechanics, Vol. 112, No. EM11, Nov. 1986, pp. 1241-1252.

7. Nogami, T. and Novak, M., 'Coefficient of Soil Reaction to Pile Vibration,' Journal of the Geotechnical Engineering Division, ASCE, Vol. 106, No. GT5, May, 1980, pp. 565-569.

8. Nogami, T.and Paulson, S.K., 'Winkler Soil Model for Axial Response Analysis of Pile Groups,' Proceedings of Symposium on Analysis and Design of Pile Foundations,' ASCE, San Francisco, California, October, 1984, pp. 287-309.

9. Nogami, T. and Paulson, S. K., 'Transfer Matrix Approach for Nonlinear Pile Group Response Analysis,' International Journal for Numerical and Analytical Methods in Geomechanics, Vol. 9, No. 4, July-August, 1985, pp. 299-316.

10. Novak, M., Nogami, T. and Aboul-Ella, F., 'Dynamic Soil Reaction for Plane Strain Case,' Journal of Engineering Mechanics Division, ASCE, Vol. 104, No. EM4, August, 1978, pp. 953-959.

11. O'Neill, M. W. and Dunnavant, T. W., 'A Study of the Effects of Seals, Velocity and Cyclic Degradability on Laterally Loaded Single Piles in Overconsolidated Clay,' Research Report UHCE 84-7, Dept. of Civil Engineering, University of Houston, 1984.

12. Sanchez Salinero, I., 'Static and Dynamic Stiffness of Single Piles,' Research Report GR82-31, Dept.of Civil Engineering, The University of Texas at Austin, 1982.